On-axis diffraction-limited bi-conical lenses

Juan Camilo Valencia-Estrada, Jorge García-Márquez

The reviewed and complete version of this paper is published in The Journal of the Optical Society of America A, Vol. 38, Issue 12, (2021). https://doi.org/10.1364/JOSAA.439565

On-axis diffraction-limited bi-conical lenses

JUAN CAMILO VALENCIA ESTRADA,[1,*] AND JORGE GARCÍA MÁRQUEZ[2]

[1] *Oledcomm, 10-12, avenue de l´Europe, Vélizy-Villacoublay, 78140, France*
[2] *Laboratoire national de Métrologie et d'Essais, Pôle Photonique - Energétique, 29, rue Roger Hennequin, Trappes, 78197, France*
[*] *camilo.valencia@oledcomm.net*

Abstract: A diffraction-limited lens having both surfaces conic is shown. The analytical and numerical calculation for all the possible solutions of the conical front and back surfaces is presented. Calculation of object and image distances, lens thickness, and refractive index is required. The process to obtain on-axis diffraction-limited images with bi-conic lenses and the proof of the method, corroborated through an example in Oslo®, is described here.

1. Introduction

Conic surfaces are used in optical systems to cope with spherical aberrations. Conical surfaces can usually appear as parabolas, ellipses, hyperbolas of revolution. However, a spherical surface is a degenerated conic. It is possible to consider flat surfaces as a conical surface's special case. A conical surface is usually represented in cylindrical coordinates (r, z) placing its vertex in the coordinate's origin while its optical axis coincides with the Z-axis: $z = c\,r^2/(1 + (1 - (1 + K)c^2\,r^2)^{1/2})$, where c is the curvature in the vertex and K a conic constant. This formulation used in geometrical optics allows for defining flat ($c = 0$), oblate elliptical ($K > 0$), spherical ($K = 0$), prolate elliptical ($-1 < K < 0$), parabolic ($K = -1$) and hyperbolic ($K < -1$) lens and mirror surfaces. Conic lenses with conical surfaces are common in everyday life. For instance, an aspheric intraocular lens (IOL) for use in a pseudophakic ocular system that has no inherent spherical aberration is disclosed in [1]; it is characterized in that two out of fourth surfaces have a conic constant that remains substantially constant over the power range of the accommodative IOL family.

The design of image forming lenses free of spherical aberration is usually performed through analytic or numerical methods. In [2] and [3], the authors show an analytical method for designing stigmatic lenses, characterized in that the lens' surfaces do not introduce spherical aberrations. We do not follow this condition here as the spherical aberration introduced by the first surface is corrected by the second surface. Of course, a combination of analytical and numerical methods is possible.

We have divided this work as follow: In the second section, we introduce the different refractive conical interfaces to design stigmatic lenses, their conic constant and respective curvature as well as their conjugated distances. In the third section, we have modelled the ray tracing and present the mathematical expressions to obtain bi-conic diffraction-limited lenses. Finally, in the fourth section, an example is solved in commercially available lens design software.

2. Common refractive conical interfaces

Conic surfaces are commonly used to avoid the introduction of spherical aberration. The choice of the conic surface depends on the combination of the conjugated object t_o and the image t_i distances. Dependence on the refractive index n is exemplified in table 1. Here, we use Descartes' sign rule to set the direction of conjugated distances.

Table 1. Refractive conic interfaces that do not introduce spherical aberration.

Conical interfaces					
Distances		Interface			
Object	Image	Surface	Curvature	Constant	Condition
Real $t_o = -\infty$	Real $t_i = +\infty$	Plane	0	0	
Virtual $t_o = R$	Real $t_i = R$	Spherical	$1/R$	0	$R > 0$
Real $t_o = R$	Virtual $t_i = R$	Spherical	$1/R$	0	$R < 0$
Virtual $t_o = (n+1)R$	Real $t_i = (n+1)R/n$	Spherical	$1/R$	0	$R > 0$
Real $t_o = (n+1)R$	Virtual $t_i = (n+1)R/n$	Spherical	$1/R$	0	$R < 0$
Real $t_o = -\infty$	Real $t_i > 0$	Ellipsoid	$n/(n-1)/t_i$	$-1/n^2$	$n > 1$
Real $t_o = -\infty$	Virtual $t_i < 0$	Ellipsoid	$n/(n-1)/t_i$	$-1/n^2$	$n > 1$
Real $t_o < 0$	Real $t_i = +\infty$	Ellipsoid	$-1/(n-1)/t_o$	$-n^2$	$0 < n < 1$
Virtual $t_o > 0$	Real $t_i = +\infty$	Ellipsoid	$-1/(n-1)/t_o$	$-n^2$	$0 < n < 1$
Real $t_o = -\infty$	Real $t_i > 0$	Hyperboloid	$n/(n-1)/t_i$	$-1/n^2$	$0 < n < 1$
Real $t_o = -\infty$	Virtual $t_i < 0$	Hyperboloid	$n/(n-1)/t_i$	$-1/n^2$	$0 < n < 1$
Real $t_o < 0$	Real $t_i = +\infty$	Hyperboloid	$-1/(n-1)/t_o$	$-n^2$	$n > 1$
Virtual $t_o > 0$	Real $t_i = +\infty$	Hyperboloid	$-1/(n-1)/t_o$	$-n^2$	$n > 1$

A clever combination of two conic surfaces (see table 1) allows designing a bi-conic stigmatic lens. For this, the first interface's image point and the second interface's object point are set to coincide. However, this condition may result in highly thick lenses. The monolithic beam-expansion element [5] is an example of thick lenses. Descartes' hyperbolic-flat lenses [6] characterizes in which the light beam in their interior is collimated. To the best of the author's knowledge, there is no analytical method used to design both conic surfaces in which one out of two conic surfaces reduces the spherical aberration introduced by the other conic surface below the diffraction limit (Fig. 1).

A vector method that corrects aberrations introduced by a surface through a correcting surface has been recently disclosed [7] and [8]. It works with any combination of conjugated planes and thickness.

Let us suppose a lens composed by a front conic surface. A back surface for correcting the first surface of intrinsic spherical aberration is required. It is possible to obtain this correcting back surface by using the method detailed in [7] by the authors. However, this back-surface solution is expressed parametrically. Thus, converting from parametric to explicit require using Taylor series, as explained in [4]. From the obtained series expansion, we look for vanishing all the deformation coefficients allowing the expansion fits a conical surface. By equaling the

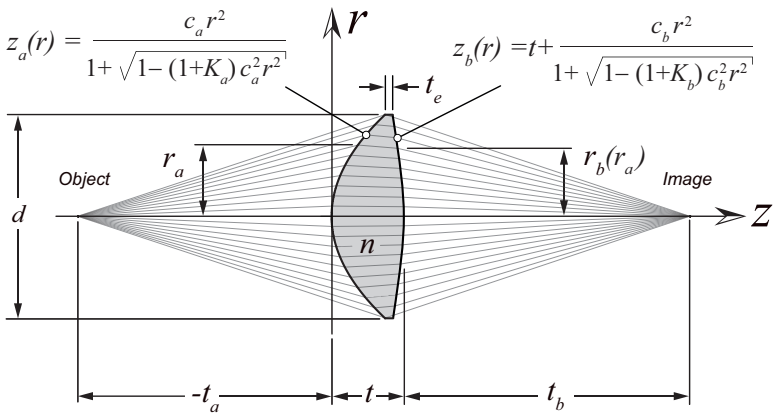

Fig. 1. Bi-conic, diffraction-limited lens. The anterior surface is $z_a(r)$, and the back surface is $z_b(r)$. Variables are c_a, K_a, c_b, and K_b are calculated. The variables t_a, t, t_b, n, and d, are prescribed. The lens' edge thickness t_e is also calculated.

4th, 6th, and 8th-degree coefficients to zero, and because of the accelerated series' convergence, finding a suitable set of conical surfaces is possible. We assume that from the 10th degree on, the coefficients have a negligible impact. Thus, for any combination of conjugated planes, a finite set of bi-conical lenses reduces spherical aberration considerably; in fact, this aberration is not only diffraction-limited but inexistent. The whole set of diffraction-limited solutions always includes the stigmatic solution; however, not always the stigmatic solution is the best one if the lens has an internal image, the lens could be damaged in its interior –for instance, it is what arrives with internal laser-based glass engraving.

3. Corrective bi-conical lenses

Let us take the anterior surface vertex as the coordinate's origin. The anterior surface z_a (sub-index a is for anterior) is a conic of revolution. In cylindrical coordinates, the conic's meridional section may be expressed as

$$z_a(r) = \frac{c_a r^2}{1+\sqrt{1-(1+K_a)\,c_a^2 r^2}}, \tag{1}$$

where K_a is the conic constant, c_a is the vertex curvature and r is the abscissa. The curvature's sign determines the surface's concavity or convexity.

The posterior surface (sub-index b is for posterior) is capable of correcting the different spherical aberration orders introduced by the anterior surface; consequently, we can represent the second surface by

$$z_b(r) = t + \frac{c_b r^2}{1+\sqrt{1-(1+K_b)\,c_b^2 r^2}} + \sum_{j=2}^{\infty} B_{2j}\, r^{2j}, \tag{2}$$

having a conical constant K_b, a vertex curvature c_b, and infinite deformation coefficients B_{2j}.

In [9], the back-correcting surface has a vertex curvature radius expressed by

$$c_b = \frac{1}{R_b} = \frac{(n-1)(t+n\,t_b)\,t_a + R_a[t+n(t_b-t_a)]}{(n-1)\,t_b[R_a(n\,t_a-t)-(n-1)\,t\,t_a]} = \frac{(n-1)(t+n\,t_b)\,c_a\,t_a + t + n(t_b-t_a)}{(n-1)\,t_b[n\,t_a-t-(n-1)\,c_a\,t\,t_a]}, \tag{3}$$

where n is the lens refraction index, $R_a = 1/c_a$ is the anterior vertex radius of curvature, $R_b = 1/c_b$ is the back vertex radius of curvature, t is the central thickness, t_a and t_b are respectively the object and the image distances as shown in Fig. 1. In this article, we only consider lenses restricted to the same refractive medium; different cases are out of scope.

Let's consider equations 5.7 to 5.12b from reference [9]. The deformation coefficients B_{2j} are analytically calculated as functions of the conic constant K_b. This deductive process is explained in the annexe of reference [4].

$$\begin{cases} B_4(K_b) = A_4 - \left(\frac{c_b}{2}\right)^3 (1+K_b), \\ B_6(K_b) = A_6 - 2\left(\frac{c_b}{2}\right)^5 (1+K_b)^2, \\ B_8(K_b) = A_8 - 5\left(\frac{c_b}{2}\right)^7 (1+K_b)^3, \\ B_{10}(K_b) = A_{10} - 14\left(\frac{c_b}{2}\right)^9 (1+K_b)^4, \\ B_{12}(K_b) = A_{12} - 42\left(\frac{c_b}{2}\right)^{11} (1+K_b)^5, \\ B_{14}(K_b) = A_{14} - 132\left(\frac{c_b}{2}\right)^{13} (1+K_b)^6, \\ \quad\vdots \\ B_{2j}(K_b) = A_{2j} - (-1)^{j+1}\,2^{2j-1}\,\mathrm{Bin}(1/2,j)\left(\frac{c_b}{2}\right)^{2j-1} (1+K_b)^{j-1}, \end{cases} \tag{4}$$

whose coefficients A_{2j} are calculated by implicitly derivation of the parametric correcting surface $\mathbf{p}_2 = [r_b(r_a), z_b(r_a)]$ [7]- [8] for the anterior explicit surface $\mathbf{p}_1 = [r_a, z_a(r_a)]$:

$$\mathbf{p}_2 = \mathbf{p}_1 + \mathbf{a}_1 = \mathbf{p}_1 + \frac{G}{V-(1-t_b)\sqrt{t_b^2\,[V^2+(n^2-1)G]}}\;\mathbf{v}_1. \tag{5}$$

where the unit vector $\mathbf{v}_1$ has the same direction of the ray propagating in the interior of the lens,

$$\mathbf{v}_1 = \frac{1}{n}[\mathbf{v}_0 - (\mathbf{n}_1 \bullet \mathbf{v}_0)\,\mathbf{n}_1] - \sqrt{1-\frac{1}{n^2}[1-(\mathbf{n}_1 \bullet \mathbf{v}_0)]}\;\;\mathbf{n}_1. \tag{6}$$

The incident unit vector $\mathbf{v}_0$ and unit normal vector $\mathbf{n}_1$ –normal to the first interface– are defined as

$$\mathbf{v}_0 = -\left.\frac{\sqrt{t_a^2}\;\mathbf{a}_0}{t_a\,\sqrt{\mathbf{a}_0 \bullet \mathbf{a}_0}}\right|_{r=r_a} = -\left.\frac{\sqrt{t_a^2}\;[r_a, z_a - t_a]}{t_a\sqrt{[r_a, z_a-t_a]\bullet[r_a, z_a-t_a]}}\right|_{r=r_a} \quad \text{and} \quad \mathbf{n}_1 = \left.\frac{\left[\frac{dz_a}{dr}, -1\right]}{\sqrt{1+\left(\frac{dz_a}{dr}\right)^2}}\right|_{r=r_a}. \tag{7}$$

Equation (5) has the following recursive variables,

$$\begin{cases} A = -t_a + \dfrac{\sqrt{t_a^2\,(r_a^2 + (z_a - t_a)^2)}}{t_a} + n\,t + t_b, \\ \\ V = (\mathbf{v}_1 \bullet \mathbf{a}_4) - n\,A = \mathbf{v}_1 \bullet [-r_a, t + t_b - z_a] - n\,A, \\ \\ G = \mathbf{a}_4 \bullet \mathbf{a}_4 - A^2 = r_a^2 + (t + t_b - z_a)^2 - A^2, \end{cases} \tag{8}$$

where $\mathbf{a}_4 = \mathbf{p}_3 - \mathbf{p}_1 = [0, t + t_b] - [r_a, z_a]$.

Equation (5) is valid for any real or virtual object-point and real or virtual image-point. In other words, it is valid for any combination of conjugated points, provided the condition $d\mathbf{p}_2/dr_a \neq [0,0]\;\forall\, r_a \subset$ aperture is fulfilled. Equation (5) is still valid in positive-magnification lenses in which all rays cross in their interior. This equation results in a long parametric solution; then we proceed to determine the deformation coefficients B_{2j} to obtain the best explicit representation. By following the procedure explained in the annexe in reference [4], coefficients A_{2j} are evaluated

$$\begin{cases} A_2 = \dfrac{1}{2!}\dfrac{d^2 z_b}{dr_b{}^2}\bigg|_{r_b=0} = \dfrac{c_b}{2}, \\ \\ A_4 = \dfrac{1}{4!}\dfrac{d^4 z_b}{dr_b{}^4}\bigg|_{r_b=0} = -\dfrac{c_b\,R_3}{6} + \dfrac{Z_4}{24}, \\ \\ A_6 = \dfrac{1}{6!}\dfrac{d^6 z_b}{dr_b{}^6}\bigg|_{r_b=0} = \dfrac{7c_bR_3^2}{72} - \dfrac{c_bR_5}{120} - \dfrac{R_3Z_4}{36} + \dfrac{Z_6}{720}, \\ \\ A_8 = \dfrac{1}{8!}\dfrac{d^8 z_b}{dr_b{}^8}\bigg|_{r_b=0} = -\dfrac{5c_bR_3^3}{72} + \dfrac{c_bR_3R_5}{80} - \dfrac{c_bR_7}{5040} + \dfrac{R_3^2Z_4}{48} - \dfrac{R_5Z_4}{720} - \dfrac{R_3Z_6}{720} + \dfrac{Z_8}{40320}, \end{cases} \tag{9}$$

with the recursive variables, R_k and Z_k defined as

$$R_k = \left.\frac{\dfrac{d^k\,r_b}{d\,r_a^k}}{\left(\dfrac{d\,r_b}{d\,r_a}\right)^k}\right|_{r_a=0} = \left.\frac{r_b{}^{(k)}}{(r_b{}')^k}\right|_{r_a=0} = \frac{r_b^{(k)}\big|_{r_a=0}}{\left[\lim\limits_{r_a\to 0}\left(\dfrac{r_b}{r_a}\right)\right]^k}, \quad \forall\, k = 3,5,7, \tag{10}$$

$$Z_k = \left.\frac{\dfrac{d^k\,z_b}{d\,r_b{}_a^k}}{\left(\dfrac{d\,r_b}{d\,r_a}\right)^k}\right|_{r_a=0} = \left.\frac{z_b^{(k)}}{(r_b{}')^k}\right|_{r_a=0} = \frac{z_b^{(k)}\big|_{r_a=0}}{\left[\lim\limits_{r_a\to 0}\left(\dfrac{r_b}{r_a}\right)\right]^k}, \quad \forall\, k = 4,6,8. \tag{11}$$

After evaluation and simplification, equations (10) and (11) are substituted into equation (9). The deformation coefficients A_{2j} in equation (9) are obtained in the limit when the abscissa r_a tends to zero; the coefficient A_2 has been used to obtain c_b in equation (3). Derivatives are evaluated in the surface's vertex. Coefficients B_{2j} are factored and fully simplified. When coefficients are equalled to zero we obtain a system with four equations and the four unknowns c_a, K_a, c_b and K_b,

$$\begin{cases} c_b = \dfrac{(n-1)(t+n\,t_b)\,c_a\,t_a + t + n(t_b - t_a)}{(n-1)\,t_b\,[n\,t_a - t - (n-1)\,c_a\,t\,t_a]}, \\ \\ B_4 = A_4 - \left(\dfrac{c_b}{2}\right)^3 (1+K_b) = 0, \\ \\ B_6 = A_6 - 2\left(\dfrac{c_b}{2}\right)^5 (1+K_b)^2 = 0, \\ \\ B_8 = A_8 - 5\left(\dfrac{c_b}{2}\right)^7 (1+K_b)^3 = 0. \end{cases} \tag{12}$$

We can obtain a reduced equations' system by substituting c_b equation (3) in the three equations for coefficients B (12b) to (12d). Next, the equations are factored in, and numerators are only considered. Finally, factors in numerators that contain the unknown variables are kept. In the case that interests us, only one factor per equation is retained.

It is possible to fit any posterior corrective aspheric surfaces, with conical constant K_b and any deformation coefficients, to a conical surface vanishing all the deformation coefficients far beyond order 10. Thus, by equaling B_4, B_6 and B_8 to zero, it is possible to find an approximation to the optimal conical surface combination because of the series' fast convergence.

Because of its extension, we recommend implementing the procedure in symbolic mathematical software. The first step is to obtain the parametric derivatives of $z_b(r_a)$ and $r_b(r_a)$ for the orders required in equation (9). $z_b(r_a)$ and $r_b(r_a)$ were defined in equation (5). The derivatives are then substituted in (12). However, the derivation's result is extremely extended, and its reduction requires factorization. The result is a polynomial division equal to zero that simplifies just retaining the polynomial's numerator. The numerator factor containing unknown variables is retained. Finally, for each equation of the system (12), their polynomial is determined. Do not evaluate the limit before the simplification process as this results in a non-consistent solution.

Next, for the unknown variables, the system of equations can be reduced to

$$\begin{aligned} 0 = {} & 4\,m^2 p\,U^2 V^3 (t_b\,U + V)^3 (t_b U + n\,V) + 4\,c_a^5\,K_a^2\,m^5 n^5 t_a^6\,t_b^4 (U-2) V\,X + n\,t_a t_b^2 (4\,\{c_a^3 K_a \\ & \times m^3\,n^2\,t_a^3\,V\,[\,t_b^2 (2\,U^3 - 4\,n\,p\,U^2 + n^2\,\{7\,n+3\}\,U - 4\,n^4)\,X - Y] + n\,t_a\,t_b^2\,Z^2\,[V+X]\} \\ & - V\,\{t_b^2\,[4\,U^3 - C]\,X - 4\,Y\}\,W), \end{aligned} \tag{13}$$

$$
\begin{aligned}
0 = &-n^3\,t_a^3\,t_b^6\,Z^3(19\,n^2\,t_b^2\,U^2+48\,n\,t_b\,U\,V+24\,V^2)-5\,m^3\,p\,U^3(t_b\,U-V)V^4(t_b\,U+V)^3\\
&\times(\{pt_b\,U+2\,V\}\,\{t_b\,U+nV\}\,\{V+n\,[2\,t_b\,U+V]\,\})+n^2\,t_a^2\,t_b^4\,V(24\,K_a^3\,n^6\,t_b^2\{Q-1\}\,Q^8\\
&\times X^2-W^2\{3\,n^2\,t_b^4\,U^2\,[2\,C+(3\,n^2-11)U^3]+2\,n\,t_b^3\,U\,[6\,C+(n\{37\,n-13\}-48)\,U^3]\\
&\times V+2\,t_b^2\,[3\,C+(n\{n\,[11\,n+57]-56\}-24)\,U^3]\,V^2+m[15n^2-n+56\,]\,t_b\,U^2V^3-8\\
&\times m\,U\,V^4\}+2K_a n^2W\,Q^3\{3\,n^2\,t_b^4U^2[4D+3(n^2-5)U^3]+2\,n\,t_b^3U[12\,D+(\{37\,n-13\}\\
&\times n-60)U^3]V+2\,t_b^2[6D+(n\{n\,[11n+57]-56\}-30)U^3]V^2+m\,[15n^2-n+56]\,t_b\\
&\times U^2V^3-8\,mUV^4+12\,n\,[n+5]p\,t_b^2U^2X^2\}-K_a^2\,n^4Q^5\{c_a m^2 t_a U\,[(n\,\{15\,n-1\}+56)\\
&\times t_b\,U-8V]V^3-t_b^2\,[3\,n^2\,t_b^2U^2(2\,E-\{n\,[37\,n+48]+35\}U^3-3\{n^2-9\}U^4)+2\,n\,t_bU\\
&\times(6E-\{n[83\,n+157]+120\}U^3-\{n[37\,n-13]-96\}U^4)V+2(3E+\{n\,[n(11\,n-3)\\
&-128]-60\}\,U^3-\{n[n(11\,n+57)-56]-48\}\,U^4)V^2]\})+n\,t_a\,t_b^2\,V^2(K_a^3\,n^6\,t_b^4\,Q^7\{5U^2\\
&-24\,U+24\}X^2-K_a^2n^4\,t_b^2\,Q^5X^2\{t_b^2[4\,n^3(30-19U)U-24(Q-1)U^3+24\,n^4(2U-3)\\
&+8\,n\,U^2(4U-7)+n^2U\,(48-99\,U+22U^2+9U^3)]+4\,m[Q-1]U\,[6\,t_bU-V]V\}-W\\
&\times\{n^2t_b^6\,U^2[A-n^3(n\{n[n(10\,n+43)+98]+99\}+10)\,U^3-n^2\,(n\,\{n\,[n\,(5\,n+2)-52]\\
&-82\}-23)U^4+n\,(2\,n-3)(5\,n+6)\,p^2U^5-(9\,n^2-14)U^6]+2\,n\,t_b^5\,U\,[A-n^3(n\,\{n\,[n\\
&\times(10\,n+19)+122]+99\}+10)U^3-n^2(n\{n[n\,(17\,n+26)-76]-94\}-23)\,U^4+n(n\\
&\times\{22n-15\}-18)p^2U^5+(3\,n\{n[n(3\,n+2)-15]+2\}+29)U^6]V+t_b^4[A-n^3(n\{n[n\\
&\times(18n-61)+194]+99\}+10)\,U^3+n^2(n\,\{n\,[n\,(n+2)(4\,n-53)+144]+130\}+23)\\
&\times U^4-n\,(n\,\{4\,n^2+51-62\,n\}+18)\,p^2U^5+(n\{n[n(n\{32n+79\}-124)-155]+144\}\\
&+29)\,U^6]V^2-2\,m\,t_b^3U^2[8(n-3)n^4-4n^2(n^3-8\,n-3)U+4(n-3)n\,p^2U^2-(n\{n\,[5n\\
&\times(3n+7)+21]-43\}-36)U^3]V^3-mt_b^2U[C-2(n\{3n^3-11n+24\}-14)U^3]V^4-24\\
&\times m^2[2n\,p+1]t_bU^3\,V^5-3m^2[5\,n+3]p\,U^2\,V^6\}-K_a n^2\,Q^3\,\{3m^2\,U^2\,V^5[8(2\,n\,p+1)\,t_bU\\
&+p\,(5\,n+3)\,V]+2\,m\,t_b^2\,U\,V^3\,[t_b\,U(16\{n-3\}n^4-4\{n-3\}n^2\{7\,n+3\}\,U+16\{n-3\}\\
&\times n\,p\,U^2-\{n\,[n\,(5\,n\{3\,n+7\}+21)-39]-48\}\,U^3)+(8n^4-2n^2\{7\,n+3\}U+8\,n\,p\,U^2\\
&-\{n[3\,n^3-11\,n+24]-12\}\,U^3)\,V]-t_b^4\,[n^2\,t_b^2\,U^2(B-4\,n^3\{n\,[6\,n^2+70\,n+101]+18\}\\
&\times U^3-2\,n^2\{n\,[n\,(22\,n-41)-150]-56\}\,U^4+4\,n\,\{n\,[3\,n\,(3\,n+2)-26\}-22\}\,U^5-3\\
&\times\{6n^2-11\}U^6)+2\,n\,t_bU(B+4n^3\{n[6\,n^2-82n-101]-18\}U^3-2n^2\{n[n(64n-65)\\
&-168]-56\}\,U^4+4\,n\,\{n[3n(7\,n+2)-38]-22\}\,U^5+3\,\{n[n(n\{3n+2\}-22)+6]+16\}\\
&\times U^6)V+(B-4\,n^3\{n[2\,n(n\{2\,n-23\}+59)+101]+18\}\,U^3+2\,n^2\{n\,[n\,(2\,n\{7\,n-99\}\\
&+131)+222]+56\}\,U^4-4\,n\,\{n\,[n(n\,\{4n-57\}-10)+74]+22\}U^5+\{n+2\}\{n\,[n\,(n\,\{32\\
&\times n+15\}-150)+84]+24\}\,U^6)V^2]\}),
\end{aligned}
\tag{14}
$$

$$R_b = -\frac{m\, t_b\, V}{X} \tag{15}$$

and

$$K_b = \frac{n[n\, t_a\, t_b^3\, Z - V(t_b\, U + V)^2(t_b\, U + n\, V)]}{V\, X^3}. \tag{16}$$

having the following local recurrent variables

$$\begin{cases} m = n - 1, \\ p = n + 1, \\ Q = c_a\, m\, t_a, \\ U = 1 + Q, \\ V = t\, U - n\, t_a, \\ W = (n - U)^2(n^2 - U), \\ X = n\, t_b\, U + V, \\ Y = m\, U\, V\, \{2\, p\, t_b^2\, U^2 + V[(3\, n + 4)\, t_b\, U + V + 2\, n\, V]\}, \\ Z = W - K_a\, n^2(U - 1)^3, \\ A = 24\, n^8 - 24\, n^6[n(n + 3) + 1]\, U + n^4[n(n\{n[5\, n + 62] + 111\} + 62) + 5]\, U^2, \\ B = 72\, n^8 - 24\, n^6[n(n + 10) + 4]\, U + n^4[2\, n(3\, n\{11\, n + 59\} + 143) + 29]\, U^2, \\ C = 8\, n^4 - 4\, n^2[n(n + 3) + 1]\, U + 4\, n\, p^2\, U^2, \\ D = 6\, n^4 - n^2[n(n + 10) + 4]\, U, \\ E = 24\, n^4 - 4\, n^2[n(5\, n + 11) + 5]\, U + 4\, n[n(9\, n + 10) + 8]\, U^2. \end{cases} \tag{17}$$

The solution of the system of equations (13) to (16) can be only obtained numerically. A code to perfom the calculations is given in reference [10]. There are 38 roots in this system of equations; some of them are real and the remaining are either imaginary or complex. The real roots correspond to the parameters of the feasible lenses. Furthermore, some real solutions could show algebraic multiplicity resulting in a reduction of feasible solutions. The existence of numerically close solutions is detected by increasing the numerical resolution in the algorithm. In addition to this, a solution may have a conic constant distant from zero, causing ray tracing instabilities to appear. Therefore, we can remove them from the set of solutions.

Additionally, some solutions cannot be manufactured for the required aperture as the intersection of both surfaces occurs for a maximum diameter $d_{max} < d$. Solutions having small or big curvature radii can also be removed. It is easy to verify that each solution's contribution to spherical aberration is remarkably insignificant. But, what about the others? Let's have a look. Aberrations vary for every different solution. For instance, some solutions have reduced coma, while others can be aplanatic. Performance of lenses as single parts of an optical system depends

on their ability to correct aberrations or image forming. Thus, the obtained solutions must be analyzed in function of their role to play in the optical system. The example in section 3 shows the whole set of found solutions that permit to understand the selection details. Assessment of this procedure may require for a ray tracing to be carried out.

4. Lens' maximun aperture diameter

The lens paraxial focal distance F is easily calculated by using the lens maker's formula,

$$\frac{1}{F} = (n-1)\Big(\frac{1}{R_a} - \frac{1}{R_b} + \frac{t}{n\,t_a\,t_b}\Big) = (n-1)\big(c_a - c_b + \frac{(n-1)\,t\,c_a\,c_b}{n}\big). \tag{18}$$

Alternatively, we can use Gullstrand's formula [11]

$$\frac{1}{F} \approx \frac{1}{t_a} + \frac{1}{t_b} + \frac{(n-1)\,t}{n\,R_a\,R_b}. \tag{19}$$

The expression relating to the diffraction-limited image requires calculating the lens aperture. To do so, we trace a marginal ray in the meridional plane to calculate the heigth $h_i(d/2)$ on the image plane. However, the marginal rays are the most aberrated of all the rays when paraxial ray tracing is used. Therefore, numerically finding the maximum aperture diameter d requires the following condition to be satisfied

$$|h_i(d/2)| \leq 1.22\lambda|F/\#| \;\text{ or }\; d|h_i(d/2)| \leq 1.22\lambda|F|. \tag{20}$$

After vanishing all the deformation coefficients in the sum of equation (2) the back surface is

$$\hat{z}_b(r) = t + \frac{c_b r^2}{1+\sqrt{1-(1+K_b)\,c_b^2 r^2}}. \tag{21}$$

The application of this equation allows for the design of bi-conical and diffraction-limited lenses for most of the market lenses' demand. Finally, the edge thickness t_e is calculated with the condition

$$t_e = \hat{z}_b(d/2) - z_a(d/2) > 0. \tag{22}$$

For a bi-conic lens design, equation (22) can be reduced to

$$t_e = t + \frac{c_b r^2}{1+\sqrt{1-(1+K_b)\,c_b^2 r^2}} - \frac{c_a r^2}{1+\sqrt{1-(1+K_a)\,c_a^2 r^2}} > 0. \tag{23}$$

5. Lens set design example

Two bi-conical diffraction-limited lenses are explained here below to exemplify this method. The lenses in Figs. 2 and 3 have the next input parameters: (i) Its object distance $t_a = -800$ (mm), (ii) its diameter $d = 5$ (mm), (iii) the image distance is $t_b = 12$ (mm), (iv) its central thickness is $t = 0.6$ (mm),it is made of glass or plastic whose refraction index is $n = 1.76$ at $\lambda = 589$ (nm). In this case 15 real and 24 complex solutions were numerically found. The subset of real solutions comprises three repeated and three unsuitable solutions because of reduced aperture diameter. In this example, thirteen different real solutions were numerically obtained as shown in table 2.

Then, two solutions 1 and 9 out of thirteen have a very high conic constant, while another seven solutions 2, 4-7, 11 and 13 have very small curvature radii. Finally, by ray tracing the four remaining feasible solutions 3, 8, 10 and 12 were evaluated; their aberrations were estimated, and their on-axis diffraction-limited image on the optical axis assessed. We have noted that smaller

Table 2. Bi-conical solutions.

Lens	$R_a = 1/c_a$	K_a	$R_b = 1/c_b$	K_b	d_{max}
1	−40.3043	−34.6289	−7.357	−2.46487	6.82111
2	−0.111131	−0.492398	−0.355761	−0.41546	∞
3	608	−3.09758	−9.12	−3.0976	6.78321
4	0.258981	−0.323328	0	−564.186	∞
5	0.259983	−0.323854	0.001004	−0.458661	∞
6	−0.268261	0.0375141	−0.49842	−0.235946	∞
7	0.46227	−0.274371	0.208177	−0.176501	∞
8	608	−0.902106	−9.12	−3.0976	6.78321
9	9.23661	−0.704097	6.45076×10^9	5.58695×10^{21}	6.62644
10	5.40373	−0.514104	12.0607	−2.44231	6.51212
11	2.97157	−0.335177	3.89039	−0.036834	6.20631
12	6.53824	−0.348457	20.9092	0.181723	6.55805
13	−1.40885	−0.636759	−1.40773	−0.694059	∞

coma appears when conic constants are closer to zero. To illustrate this, we show the ray tracing for two solutions 12 and 3 out of four selected solutions.

In figure 2 an elliptic oblate spheroid lens with curvature radii $R_a = 6.538235$ (mm), and $R_b = 20.909229$ (mm), conic constants $K_a = -0.348456698$, and $K_b = 0.181723306$ is shown. We introduce these values in OSLO® (a lens design software) to verify [Fig 2(a)] that the image is diffraction limited for a $F/\# = 2.49$ [Fig 2(b)]. An object point with height $h_o = -100$ (mm) is imaged with a negative coma, as shown in Fig. 2(c). The anterior sagitta calculation: $s_a = 0.489917$ (mm) is required for coupling the diaphragm to the surface. The lens' effective focal length is $F = 12.295271$ (mm). We can compare now this result with the result for a bi-parabolic as reported in [4]. Spherical aberration is smaller when the lens is bi-conical even if in both cases the spherical aberration is below the diffraction-limit. For comparative purposes, the same entrance parameters t_a, t, t_b, n, and d were used.

This example is easily assessed by using any optical design software by taking care the following steps: a) Compute R_a, K_a, R_b and K_b by solving numerically the equations' system (13) to (16) using the recurrent variables (17); b) choose convenient solutions according to the designing specifications. Then, for each selected lens, c) calculate the focal distance F by using equations (18) or (19). d) Equation (20) allows determining the maximum aperture diameter by ensuring a diffraction-limited image. e) The edge thickness t_e calculated with equation (23) should meet the condition given. However, if $t_e < 0$, then the central thickness t increases, implying the repetition of all the steps.

The solution shown in figure 3 corresponds to a bi-hyperbolic lens with curvature radii $R_a = 608$ (mm), and $R_b = -9.12$ (mm), and conic constants $K_a = K_b = -3.0976 = -n^2$. This classical stigmatic solution, obtained according to parameters in table 1, appear when the internal rays are collimated. For assessing purposes, we introduce these values in Oslo® again and verify [Fig 2(a)] that the image is diffraction-limited for a $F/\# = 2.40$, [Fig 3(b)]. Then, in Fig. 3(c), the coma aberration in the image plane is depicted; however, a bigger coma

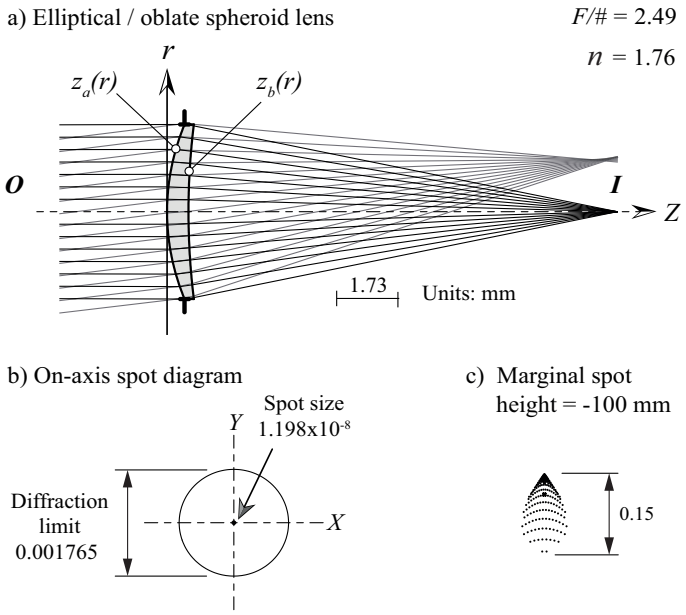

Fig. 2. On-axis diffraction-limited elliptical/oblate spheroid lens. (a) On-axis and tilted beams.The object and the Gaussian image heights are $h_o = -100$ (mm) and $h_i = 1.5612$ (mm). Geometrical spots in Figs. (b) and (c) and diffraction-limit circle (b) are expressed in mm, and the reference wavelength is $\lambda = 589$ (nm). These results were assessed in Oslo®.

appears. Its corresponding object point is placed at a height $h_o = -100$ (mm). In this case, the coma is positive. Coupling the diaphragm with the surface implies anterior sagitta calculation $s_a = 0.005141$ (mm). The lens' effective focal length is $F = 11.827627$ (mm). Now, it is possible to compare this result with the bi-parabolic lens reported in [4]. For the same entrance parameters t_a, t, t_b, n, and d we can observe that spherical aberration is smaller in bi-conical lenses than in a bi-parabolic lens, being both of them diffraction-limited. However, the coma is worsening compared with the lens in the example shown in Fig. (2).

Let us now consider a different set of entrance parameters: (i) The object distance is $t_a = -800$ (mm), (ii) the diameter is $d = 5$ (mm), (iii) the mage distance is $t_b = 3.5$ (mm), (iv) the lens central thickness $t = 1.3$ (mm), (v) image distance $t_b = 3.5$ (mm); the lens is made of the same material whose refraction index $n = 1.76$ at $\lambda = 589$ (nm). The solution corresponds to an elliptic/oblate spheroid lens as shown in Fig. 4. The lens's curvature radii are $R_a = 2.370963$ (mm), and $R_b = 5.341357$ (mm), with the following conic constants $K_a = -0.332379617$, and $K_b = 0.10331565$. Next, we assess these values in Oslo®to verify -in Fig. 4(a)- that the image is diffraction-limited when the $F/\# = 0.93$ -Fig. 4(b). When the object has a height $h_o = -100$ (mm) its corresponding coma aberration is negative as depicted in Fig. 4(c). Coupling the diaphragm with the surface implies anterior sagitta $s_a = 1.748427$ (mm). The lens' effective focal distance is $F = 4.661162$ (mm). This example clearly shows the design feasibility of fast ($F/\# < 1$) bi-conic lenses limited by diffraction.

6. Conclusions

Here, we have followed essentially the same method as the one reported previously in [4]. We have generalised the method to coefficients B_4, B_6, and B_8. The generalization has the next advantages: First, it allows to obtain an image limited by diffraction as a consequence of the fast convergence

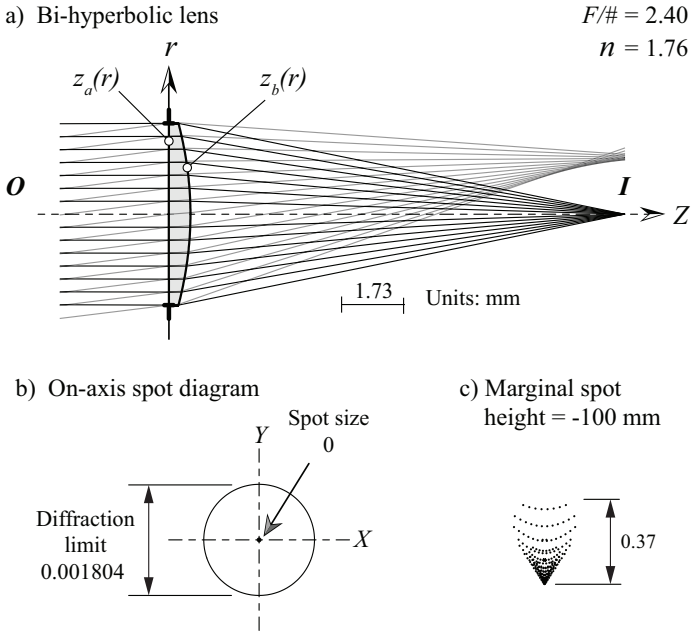

Fig. 3. On-axis diffraction limited bi-hyperbolic lens. (a) Ray tracing is shown for on-axis and tilted beams. The object and the Gaussian image heights are respectively h_o = 100 (mm) and h_i = 1.5 (mm). Geometrical spots dimensions are presented in Figures (b) and (c). The spot size and the diffraction limit circle (b) are in millimeters; the reference wavelength is λ = 589 (nm). These results were assessed in Oslo®.

of the deformation series in the approximation expressed by Eq.(2). Our assumption that the 10th degree or higher-order coefficients has an insignificant impact on the image proved to be well-founded. Second, it allows for basic optical systems design simplification by using aspheric lenses. Third, bi-conical lenses can be used to design confocal systems, i.e., systems where a diffraction-limited image point acts as the following element object point. Every combination of conjugated plane's distances involves several optimal design solutions; and finally, iv) fast bi-conic lenses design has been confirmed.

Simulations allow concluding that in bi-conical lenses, coma could be lower than coma due to spherical lenses. Nevertheless, following an applicative design, field curvature and astigmatism may increase. In addition to that, the ghost image due to internal reflections and refractions impedes obtaining a perfect image. A ray-tracing simulation was performed in Oslo® for methodology assessment; neither the optimization nor the defocus was incurred. Bi-conic lenses' aberration theory is still an open domain [12]. We hope that this result allows enhancing aspheric lenses metrology methods [13] and eye's modelling. and eye modeling. A coding program developed Mathematica® is included as supplementary material [10].

Ethics statement

This work did not involve any activity collection of human data, neither computer simulation of human behavior.

Data accessibility statement

This work does not have any experimental data.

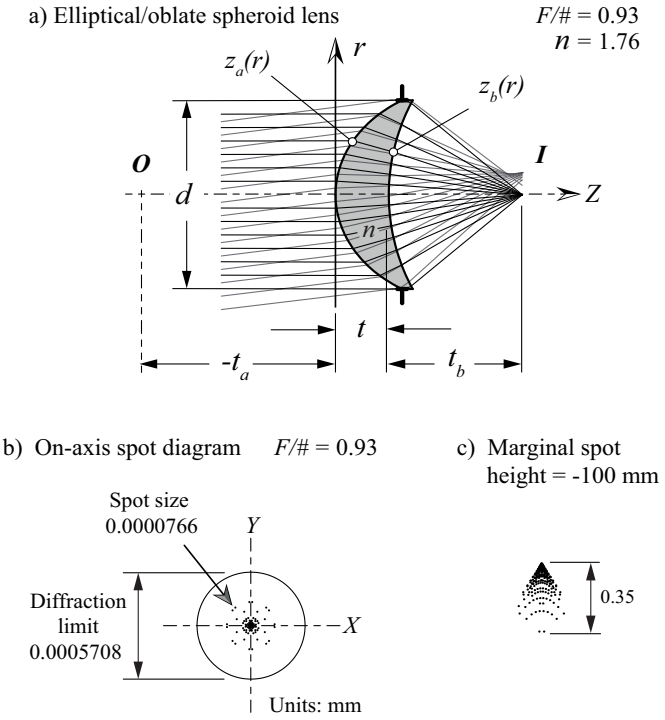

Fig. 4. On-axis diffraction limited elliptical/oblate spheroid lens. (a) Ray tracing is shown for on-axis and tilted beams. The object and the Gaussian image heights are respectively $h_o = -100$ (mm) and $h_i = 0.586449$ (mm). Geometrical spots dimension (b and c) and diffraction limit (b) are in millimeters for a reference wavelength $\lambda = 589$ (nm). These results were assessed in Oslo®.

Disclosures

The authors declare no conflicts of interest. Both authors developed the physical model and programming. All authors gave final approval for publication.

Data availability

No data were generated or analyzed in the presented research.

References

1. G. E. Altmann, “Aspheric lenses and lens family,” US 7905917 (B2), European Patent Office, (15th March 2011), Assignee: Bausch & Lomb Incorporated.
2. Silva-Lora A. and Torres R., "Superconical aplanatic ovoid singlet lenses," *J. Opt. Soc. Am. A* **37**, 1155-1165 (2020). doi.org/10.1364/JOSAA.35.001385.
3. Silva-Lora A. and Torres R., "Rigorously aplanatic Descartes ovoids," *J. Opt. Soc. Am. A* **38**, 1160-1169 (2021). doi.org/10.1364/JOSAA.422809.
4. Valencia-Estrada J.C. and García-Márquez J. "On-axis diffraction-limited design of bi-parabolic singlet lenses," *Optik***193**, 162970 (2019). doi:10.1016/j.ijleo.2019.162970.
5. Fuchs U. "New Dimensions in Beam Expansion: New add-on element allows usage over broad wavelength range," *Optik & Photonik* **10**, 39-42. (2015). doi:10.1002/opph.201500013.
6. Descartes R. *Discours de la méthode pour bien conduire sa raison el chercher la vérité dans les sciences, with three appendices: La Dioptrique*. Leyden, Netherlands (1637).
7. Valencia-Estrada J.C. and García-Márquez J. "Freeform geometrical optics I: Principles," *Applied Optics* **58**(34), 9455-9464 (2019). doi:10.1364/AO.58.009455.

8. Grillon T.M.J, Valencia-Estrada J.C. and García-Márquez J. "Freeform geometrical optics II: From parametric representation to CAD/CAM;" *Applied Optics* **58**(34), 9465-9472 (2019). doi:10.1364/AO.58.009465.
9. Valencia-Estrada J.C., Florez-Hernández R. and Malacara-Hernández D. "Singlet lenses free of all orders of spherical aberration," *Proceedings of Royal Society A* **471**, 20140608 (2015). doi:10.1098/rspa.2014.0608.
10. Code to calculate all on-axis diffraction-limited bi-aspheric lenses with conical surfaces. https://hal.archives-ouvertes.fr.
11. Gullstrand A. *Allgemeine Theorie der Monochromatischen Aberrationen und ihre nächsten Ergebnisse für die ophthalmologie*. Salzwasser Verlag, Paderborn (2012).
12. Zhong Y. and Gross H. "Vectorial aberrations of bi-conic surfaces," *J. Opt. Soc. Am. A* **35**(8), 1385-1392 (2018). doi.org/10.1364/JOSAA.35.001385.
13. Tellez-Quiñones A., Malacara-Doblado D. and García-Márquez J. "Differentiability of a projection functional in ray-tracing processes: applied study to estimate the coefficients of a single lens with conic surfaces," *J. Opt. Soc. Am. A* **32**(1), 35-45 (2015). doi:10.1364/JOSAA.32.000035.

(* Biconical lenses 8/1/2019 *)
(* Juan Camilo Valencia and Jorge Garcia Marquez *)
(* Code developed to run in Mathematica™ *)

Input:

```
Clear["Global`*"]
Print["Resolution                = " , res=100]
Print["Object distance           = " , ta=-800]
Print["Center thickness          = " , t=0.6]
Print["Image distance            = " , tb=12]
Print["Refractive index          = " , n=1.76]
m =n-1;
p = n+1;
Q = ca m ta;
U = Q+1;
V = t U -n ta;
W = (n-U)^2 (n^2-U);
X = n tb U+V;
Y = m U V (2 p tb^2 U^2+V ((3 n+4) tb U+V+2 n V));
Z = W-Ka n^2 (U-1)^3;
A = 24 n^8-24 n^6 (n (n+3)+1) U+n^4 (n (n (n (5 n+62)+111)+62)+5) U^2;
B = 72 n^8-24 n^6 (n (n+10)+4) U+n^4 (2 n (3 n (11 n+59)+143)+29) U^2;
Cc = 8 n^4-4 n^2 (n (n+3)+1) U+4n p^2 U^2;
Dd = 6 n^4- n^2 (n (n+10)+4) U;
Ee = 24n^4-4 n^2 (n (5 n+11)+5) U+4 n (n (9 n+10)+8) U^2;

(* EQUATIONS *)
sols=Quiet[NSolve[{
0== 4m^2 p U^2 V^3 (tb U+V)^3 (tb U+n V)+4ca^5 Ka^2 m^5 n^5 ta^6 tb^4 (U-2) V X+n ta tb^2 (4(ca^3 Ka m^3 n^2 ta^3 V (tb^2 (2 U^3-4 n p U^2+n^2 (7 n+3) U-4 n^4) X-Y)+n ta tb^2 Z^2 (V+X))-V (tb^2 (4U^3-Cc) X-4 Y) W),

0== -n^3 ta^3 tb^6 Z^3 (19 n^2 tb^2 U^2+48 n tb U V+24 V^2)- 5 m^3 p U^3 (tb U-V) V^4 (tb U+V)^3 ((p tb U+2 V) (tb U+n V) (V+n (2 tb U+V))) +n^2 ta^2 tb^4 V (24 Ka^3 n^6 tb^2 (Q-1) Q^8 X^2-W^2 (3 n^2 tb^4 U^2 (2 Cc+(3 n^2-11) U^3)+2 n tb^3 U (6 Cc+( n (37 n-13)-48) U^3) V+2 tb^2 (3 Cc+(n (n (11 n+57)-56)-24) U^3) V^2+m (15 n^2-n+56) tb U^2 V^3-8 m U V^4)+ 2 Ka n^2 W Q^3 (3 n^2 tb^4 U^2 (4 Dd+3 (n^2-5) U^3)+2 n tb^3 U (12 Dd+((37 n-13) n-60) U^3) V+2 tb^2 (6 Dd+(n (n (11 n+57)-56)-30) U^3) V^2+ m (15 n^2-n+56) tb U^2 V^3-8 m U V^4+12 n (n+5) p tb^2 U^2 X^2)-Ka^2 n^4 Q^5 (ca m ^2 ta U ((n (15 n - 1 )+56) tb U-8 V) V^3-tb^2 (3 n^2 tb^2 U^2 (2 Ee-(n (37 n+48)+35) U^3-3 (n^2-9) U^4)+2 n tb U (6 Ee - (n (83 n+157)+120) U^3-(n (37 n-13)-96) U^4) V+2 (3 Ee+(n (n (11 n-3)-128)-60) U^3-(n (n (11 n+57)-56)-48) U^4) V^2)))+n ta tb^2 V^2 (Ka^3 n^6 tb^4 Q^7 (5 U^2-24 U+24) X^2-Ka^2 n^4 tb^2 Q^5 X^2 (tb^2 ( 4 n^3 (30 -19 U) U-24 (Q-1) U^3+24 n^4 (2 U-3)+8 n U^2 (4 U-7)+n^2 U (48-99 U+22 U^2+9 U^3)) +4 m (Q-1) U (6 tb U-V) V)-W (n^2 tb^6 U^2 (A-n^3 (n (n (n (10 n+43)+98)+99)+10) U^3-n^2 (n (n ( n (5 n+2)-52)-82)-23) U^4+n (2 n-3) (5 n+6) p^2 U^5-(9 n^2-14) U^6)+2 n tb^5 U (A-n^3 (n (n (n (10 n +19)+122)+99)+10) U^3-n^2 (n (n (n (17 n+26)-76)-94)-23) U^4+n (n (22 n-15)-18) p^2 U^5+(3 n (n ( n (3 n +2)-15)+2)+29) U^6) V+tb^4 (A-n^3 (n (n (n (18 n-61)+194)+99)+10) U^3+n^2 (n (n (n (n +2) (4 n-53)+144)+130)+23) U^4-n (n (4 n^2+51-62 n)+18) p^2 U^5+(n (n (n (n (32 n+79) -124)-155) +144)+29) U^6) V^2-2 m tb^3 U^2 (8 (n-3) n^4-4 n^2 (n^3-8 n-3) U+4 (n-3) n p^2 U^2-(n (n (5 n (3 n +7) +21)-43)-36) U^3) V^3- m tb^2 U ( Cc-2(n (3 n^3-11 n+24)-14) U^3) V^4-24 m^2 (2 n p +1) tb U^3 V^5-3 m^2 (5 n+3) p U^2 V^6)-Ka n^2 Q^3 (3 m^2 U^2 V^5 (8 (2 n p+1) tb U+p (5 n+3) V)+2
```

```
m tb^2 U V^3 (tb U (16 (n-3) n^4-4 (n-3) n^2 (7 n+3) U+16 (n-3) n p U^2-(n (n (5 n (3 n+7)+21)-39)-48) U^3)+(8 n^4- 2 n^2 (7 n+3) U+8 n p U^2-(n (3 n^3-11 n+24)-12) U^3) V)-tb^4 (n^2 tb^2 U^2 (B-4 n^3 (n (6 n^2+70 n+ 101)+18) U^3-2 n^2 (n (n (22 n-41)-150)-56) U^4+4 n (n (3 n (3 n+2)-26)-22) U^5-3 (6 n^2-11) U^6)+2 n tb U (B+4 n^3 (n (6 n^2-82 n-101)-18) U^3-2 n^2 (n (n (64 n-65)-168)-56) U^4+4 n (n (3 n (7 n +2)-38)-22) U^5+3 (n (n (n (3 n+2)-22)+6)+16) U^6) V+(B-4 n^3 (n (2 n (n (2 n-23)+ 59)+ 101)+18) U^3+2 n^2 (n (n (2 n (7 n-99)+131)+222)+56) U^4-4 n (n (n (n (4 n-57)-10)+ 74)+ 22) U^5+ (n+2) (n (n (n (32 n+15)-150)+84)+24) U^6) V^2)))}, {Ka, ca}, res]];
Print["Real and complex solutions           = " , Length[sols]]
k = 1;
solreal = {};
Do[Kaa = Ka/.sols[[j,1]];caa = ca/.sols[[j,2]];
        If[Im[Kaa] == 0 && Im[caa] == 0,
        Clear[ca, Ka];
        solreal = Append[solreal,{k, 1/caa, Kaa,rbb=(-((m tb V)/X))/.{ca → caa, Ka → Kaa},
        Kbb = (1/(V X^3) n (n ta tb^3 Z-V (tb U+V)^2 (tb U+n V)))/.{ca → caa, Ka → Kaa}}];
        k++], {j, 1, Length[sols]}];
Print["Real solutions       = " , Lr = Length[solreal]]
Print["" ]

Print["REAL SOLUTIONS" ]
Print["{Position, Anterior radius, Anterior conical constant, Back radius, Back conical constant}" ]
Do[Print[Round[solreal[[kk]],0.0000000001]], {kk,1,Lr}]
(* Maximmun aperture calculation *)
Print["" ]
Print["Aperture calculations" ]
Print["{Position, Radial aperture}" ]
Do[Print[{kk, NSolve[ r^2/(solreal[[kk, 2]](1+Sqrt[1-(1+solreal[[kk, 3]])(r/solreal[[kk, 2]])^2 ]))==t+r^2/(solreal[[kk, 4]](1+Sqrt[1-(1+solreal[[kk, 5]])(r/solreal[[kk, 4]])^2])), {r}]}], {kk, 1, Lr}]
```

Output:

```
Resolution                  = 100
Object distance             = -800
Center thickness            = 0.6
Image distance              = 12
Refractive index            = 1.76
Real and complex solutions  = 39
Real solutions              = 15

REAL SOLUTIONS

{Position, Anterior radius, Anterior conical constant, Back radius, Back conical constant}

{1., -40.3043, -34.6289, -7.357, -2.46487}
{2., -0.111131, -0.492398, -0.355761, -0.41546}
{3., 608., -3.09758, -9.12, -3.0976}
{4., 0.258981, -0.323328, 0, -564.186}
{5., 0.258981, -0.323328, 0, -564.186}
```

{6., 0.258981, -0.323328, 0, -564.186}
{7., 0.259983, -0.323854, 0.00100359, -0.458661}
{8., -0.268261, 0.0375141, -0.49842, -0.235946}
{9., 0.46227, -0.274371, 0.208177, -0.176501}
{10., 608., -0.902106, -9.12, -3.09761}
{11., 9.23661, -0.704097, 6.45076×10^{9}, 5.58695×10^{21}}
{12., 5.40373, -0.514104, 12.0607, -2.44231}
{13., 2.97157, -0.335177, 3.89039, -0.036834}
{14., 6.53824, -0.348457, 20.9092, 0.181723}
{15., -1.40885, -0.636759, -1.40773, -0.694059}

Aperture calculations

{Position, Radial aperture}

{1, {{r→-3.41055}, {r→3.41055}}}
{2, {{r→0. +2.68097 i}, {r→0. -2.68097 i}}}
{3, {{r→3.3916}, {r→-3.3916}}}
{4, {}}
{5, {}}
{6, {}}
{7, {{r→0. +1.7594 i}, {r→0. -1.7594 i}}}
{8, {}}
{9, {}}
{10, {{r→-3.3916}, {r→3.3916}}}
{11, {{r→-3.31322}, {r→-3.31322}, {r→3.31322}, {r→3.31322}}}
{12, {{r→0. +10.0046 i}, {r→0. -10.0046 i}, {r→-3.25606}, {r→3.25606}}}
{13, {{r→-3.10316}, {r→3.10316}}}
{14, {{r→-3.27903}, {r→3.27903}}}
{15, {{r→3.41013 +0.289293 i}, {r→3.41013 -0.289293 i}, {r→-3.41013+0.289293 i}, {r→-3.41013-0.289293 i}}}